



Sub-1 min Sinter-Bonding Technique in Air Using Modified Cu Dendritic Particles for Formation of a High-Temperature Sustainable Bondline

Eun Byeol Choi¹ · Jong-Hyun Lee²

Received: 22 April 2020 / Accepted: 21 June 2020
© The Korean Institute of Metals and Materials 2020

Abstract

A pressure-assisted sinter-bonding technique in air using modified Cu dendritic particles is suggested to obtain a high-temperature sustainable bondline for wide band-gap power devices. The combination of void filling by the bending deformation of stems in the dendritic particles, prompt sintering of nanonodules on the surfaces of the particles, and generation of fresh Cu by in situ reduction on surfaces of the particles exhibited extremely rapid sinter bonding. A die attached under 10 MPa for 10 s at 300 °C and under 5 MPa for 60 s at 350 °C demonstrated shear strength of 26.2 and 20.6 MPa, respectively, surpassing that of a die attached using Pb–5Sn.

Keywords Cu dendritic particle · Sinter-bonding · Bending deformation · Nanonodule · Shear strength

1 Introduction

As electric vehicles replace those with combustion-engines, alternative bonding technologies without solder have been recently researched for high-temperature operating devices such as insulated-gate bipolar transistors [1, 2]. In such applications, the formation of bondlines compatible with high temperatures up to 300 °C is urgently required as Si is expected to be gradually replaced with wide-bandgap semiconductor materials, such as SiC, which provide higher power densities and lower switching losses at higher temperatures [3, 4].

Sinter bonding using pastes that include Ag particles, which exhibit high remelting point and thermal conductivity, has enabled pressureless techniques or sinter-bonding temperatures lower than the soldering temperatures of high-Pb solders [5–8]. However, inherently high material costs,

long bonding time, and ion migration characteristics still delay the commercialization of these technologies. Hence, various sinter-bonding methods using Cu as an alternative material are gaining more attention despite its susceptibility to oxidation. As such, Cu sinter bonding has been conducted by suppressing the Cu oxidation using a reducing or vacuum atmosphere [9–14]. Nevertheless, the use of nanoparticles [9–11, 13, 14] and the long bonding time [12, 13] are still problematic for industrial applications. For example, pressure-assisted sinter bonding for 5 min in each atmosphere, to the best of our knowledge, has produced successful results [9, 10, 14].

Therefore, we adopted uniquely-shaped Cu dendritic particles with nano-sized nodules on their surfaces as effective Cu filler in this study, to achieve rapid sinter bonding below 1 min with assistance of their large surface area. As a criterion for the achievement of rapid sinter bonding, the shear strength (~20 Mpa) of Pb–5Sn bondlines was adopted [15].

2 Experimental Procedure

The modified Cu dendritic particles (WFDR-4, D50: 3.8 μm) with short branch length, synthesized through a wet method, were supplied by Epsilon Epowder (Seongnam-City, Korea) [16]. The morphologies of the prepared Cu particles were examined using a high-resolution field-emission scanning

✉ Jong-Hyun Lee
pljh@snut.ac.kr

¹ Program of Materials Science and Engineering, Convergence Institute of Biomedical Engineering and Biomaterials, Seoul National University of Science and Technology, Seoul 01811, Republic of Korea

² Department of Materials Science and Engineering, Seoul National University of Science and Technology, Seoul 01811, Republic of Korea

electron microscope (HR-SEM, SU8010, Hitachi), and the average size was measured using a laser particle size analyzer (PSA, S3500, Microtrac). Phase identification of initial particles and phase changes in bondlines after air heating for sinter bonding were analyzed using an X-ray diffractometer (XRD, DE/D8 Advance, Bruker). The bondline was prepared by cross-sectional polishing after mounting a sinter-bonded sample. To evaluate the heat-flow status and weight change of the Cu particles as well as a Cu paste upon heating to 400 °C in air, thermogravimetry (TG, DTG-60, Shimadzu) and differential scanning calorimetry (DSC, DSC-60, Shimadzu) analyses were conducted at a heating rate of 10 °C/min.

Pastes containing the Cu dendritic particles were prepared by mixing them with a reduction formulation developed in-house as a vehicle with a particle-to-vehicle weight ratio of 55:45. A dummy Cu die of volume $3 \times 3 \times 1 \text{ mm}^3$ was sinter-bonded on a dummy Cu substrate of volume $10 \times 10 \times 1 \text{ mm}^3$. The dummies were polished using 2000-mesh sandpaper. Then, they were etched for 3 min using 90 ml of ethanol (95%, Korea Alcohol Industrial Co., Ltd.)/10 ml of sulfuric acid (98%, Daejung Chemicals & Metals Co., Ltd.) solution. After rinsing with ethanol and drying, the prepared paste was printed onto the substrate through a stencil mask with a $3 \times 3 \times 0.1\text{-mm}^3$ slit. Subsequently, the die was placed on the printed pattern and slightly dried for 30 s at 150 °C on a hot plate. Lastly, the sandwich-structured sample was heated in air up to 300–350 °C for the die attachment using a thermo-compression bonder. Pressure of 2–10 MPa was automatically maintained throughout the bonding time from

the start of heating. The sinter-bonding characteristics were evaluated as a function of bonding time as well as bonding temperature. A schematic of the sinter-bonding process is presented in Fig. 1.

The microstructures of the bondlines after bonding and the fracture surfaces after shear testing were observed using HR-SEM. The bonding strength of the bondline was defined as an average value of the maximum stress values measured during the shear testing of ten samples with a speed of 200 $\mu\text{m/s}$ at a shear-tip height of 200 μm above the substrate surface.

3 Results and Discussion

Figure 2a, b show the low and high-magnification images of the Cu dendritic particles. The particle morphology was a rice-ear shape comprising sea-cucumber-like aggregates of Cu nanoparticles. Thus, nano-sized nodules were observed on the surfaces of the aggregates (inset of Fig. 2b). Despite their large surface area, the Cu oxide peaks were scarcely observed in the XRD measurement (Fig. 2c) with meticulous post-treatment after wet synthesis. The TG-DSC results of the Cu dendritic particles in air are displayed in Fig. 2d. The oxidation weight increase began at 151 °C, and the first oxidation exothermic peak was measured at 183 °C, a temperature lower than that of similarly-sized, spherical Cu particles due to the significantly increased surface area [17]. However, completely different results were measured in the Cu paste containing a reduction formulation (Fig. 2e); the

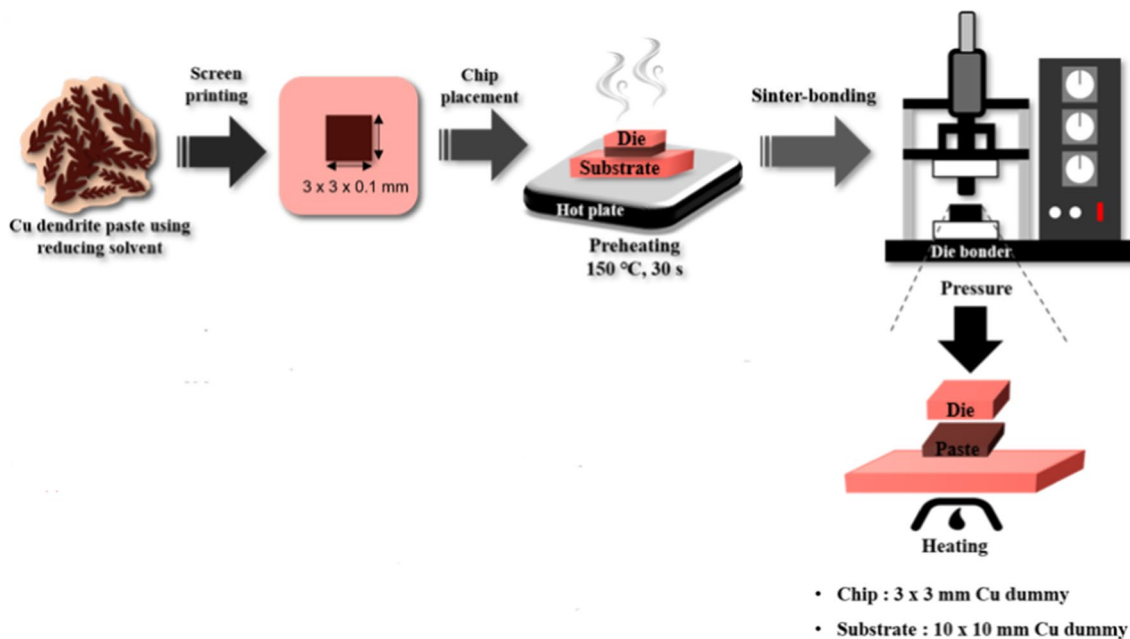
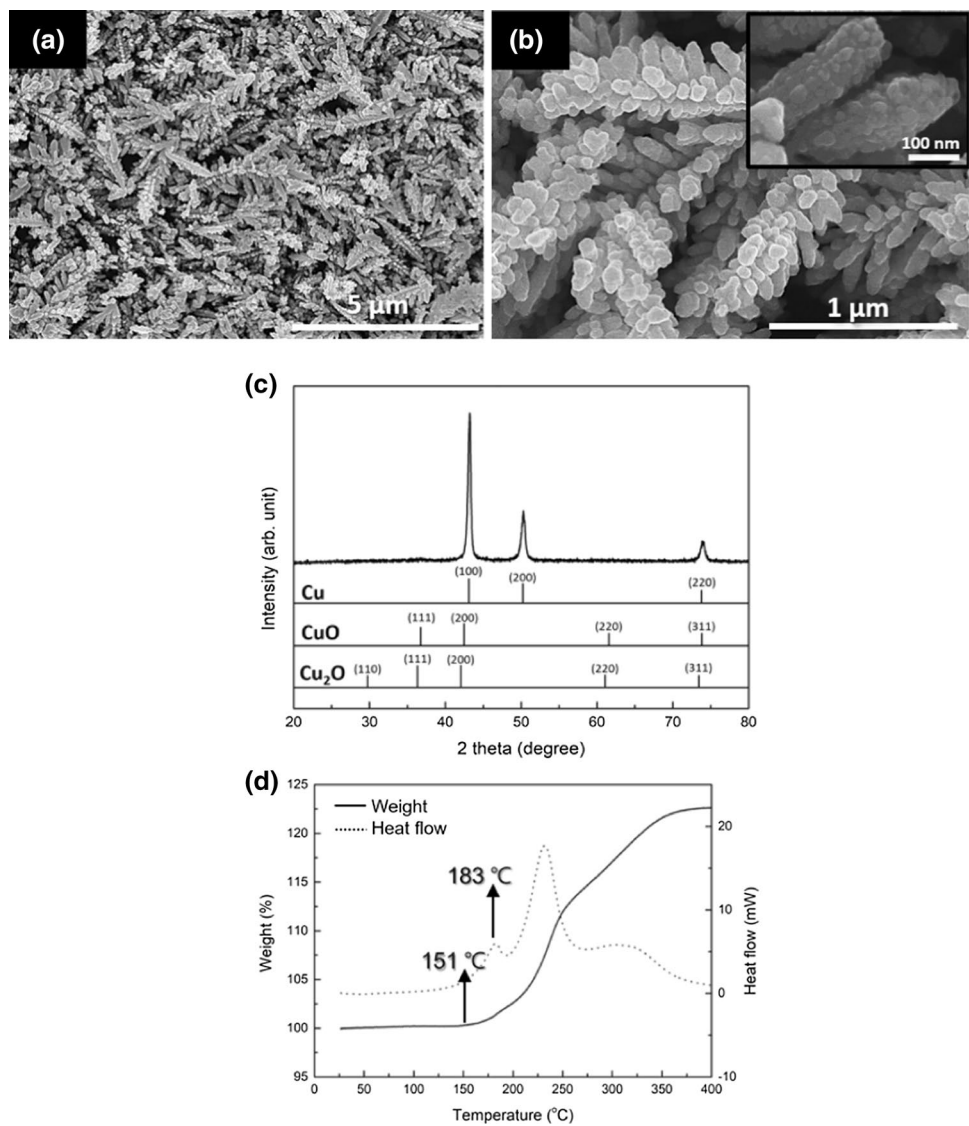


Fig. 1 Schematic of the sinter-bonding process

Fig. 2 a, b SEM images, c XRD result, and TG-DSC results of d Cu dendritic particles and e Cu paste containing a reduction formulation



weight decreased until a temperature of 227 °C was reached and then increased from 267 °C due to oxidation. Furthermore, a new endothermic peak was observed at 201 °C; the exothermic peak was delayed to 224 °C. The endothermic peak was attributed to reduction on the surfaces of Cu dendritic particles due to their formulation. Therefore, the surfaces oxidized in the paste during heating to nearly 200 °C were anticipated to be reduced at approximately 200 °C. Although the Cu particles reoxidize at higher temperatures in air even after reduction, the oxidation may be significantly suppressed if the particles are rapidly sintered into a dense microstructure with the assistance of external pressure.

The measured heating profiles for sinter bonding are displayed in Fig. 3. When heated to 300 °C (Fig. 3a), the temperature was attained after 10 s. Thus, the bonding conditions for 10 s at 300 °C imply that temperature in the bondline just approached 300 °C. Meanwhile, when heated to

350 °C (Fig. 3b), the temperature was reached after 30 s. Therefore, the 10 s heating at 350 °C implies that temperature in the bondline was only 320 °C.

Figure 4a exhibits the average shear strength of bondlines sinter-bonded with different combinations of process parameters. Under a pressure of 2 MPa, sinter bonding at 350 °C indicates that the strength increases proportionally with increasing bonding time. As a result, the strength reaches 23.0 MPa after 5 min, which is higher than that of Sn-5Pb (20 MPa). With a pressure increase to 5 MPa, the 300 °C sinter-bonding strength approached 20 MPa (19.0 MPa) after 3 min. Moreover, the 350 °C bonding produced strength exceeding 20 MPa (20.6 MPa) after only 60 s. Hence, it was concluded that higher pressure and temperature accelerate sinter bonding. The increased pressure of 10 MPa significantly enhanced the sinter bondability; the 300 °C sinter bonding achieved a sufficient strength of 26.2 MPa after 10

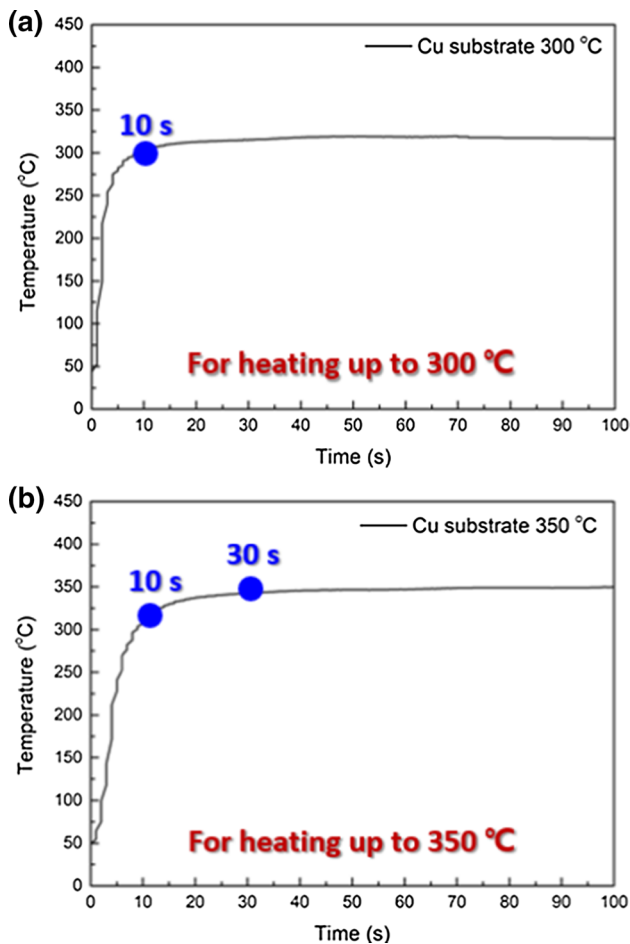


Fig. 3 Heating profiles for sinter bonding at **a** 300 °C and **b** 350 °C

s and enhanced the strength up to 31.7 MPa after 60 s. The sinter bonding at 250 °C reached a strength of 25.1 MPa after 30 s.

Among the XRD patterns (Fig. 4b) of the bondlines obtained after sinter heating with different conditions, a slight Cu_2O phase was detected in most cases. Bonding for 1–5 min at 350 °C indicated the formation of Cu oxide phase(s). Meanwhile, bonding at 300 °C showed distinct Cu_2O formation only after the extended bonding time of 5 min; however, the phase was barely detected immediately after 60 s. When bonding at 250 °C, Cu_2O was scarcely detected even after 5 min. These results imply that the degree of oxidation is strongly dependent on bonding temperature and time, rather than pressure. While the bonding conditions of 3 min at 300 °C and 60 s at 350 °C under 5 MPa created a slight presence of Cu oxide, the conditions of 10 s at 300 °C under 10 MPa did not, implying that extremely rapid sinter bonding suppresses the oxidation of Cu filler particles. While the oxidation degree in a bondline was mainly influenced by bonding temperature and time, the bondline is anticipated to indicate excellent thermal conductivity as

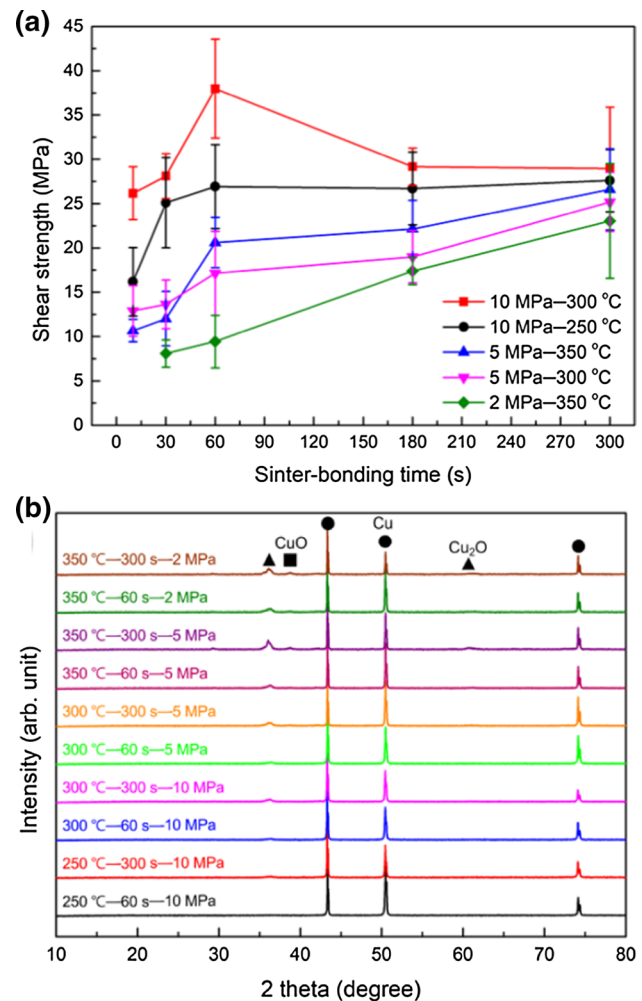
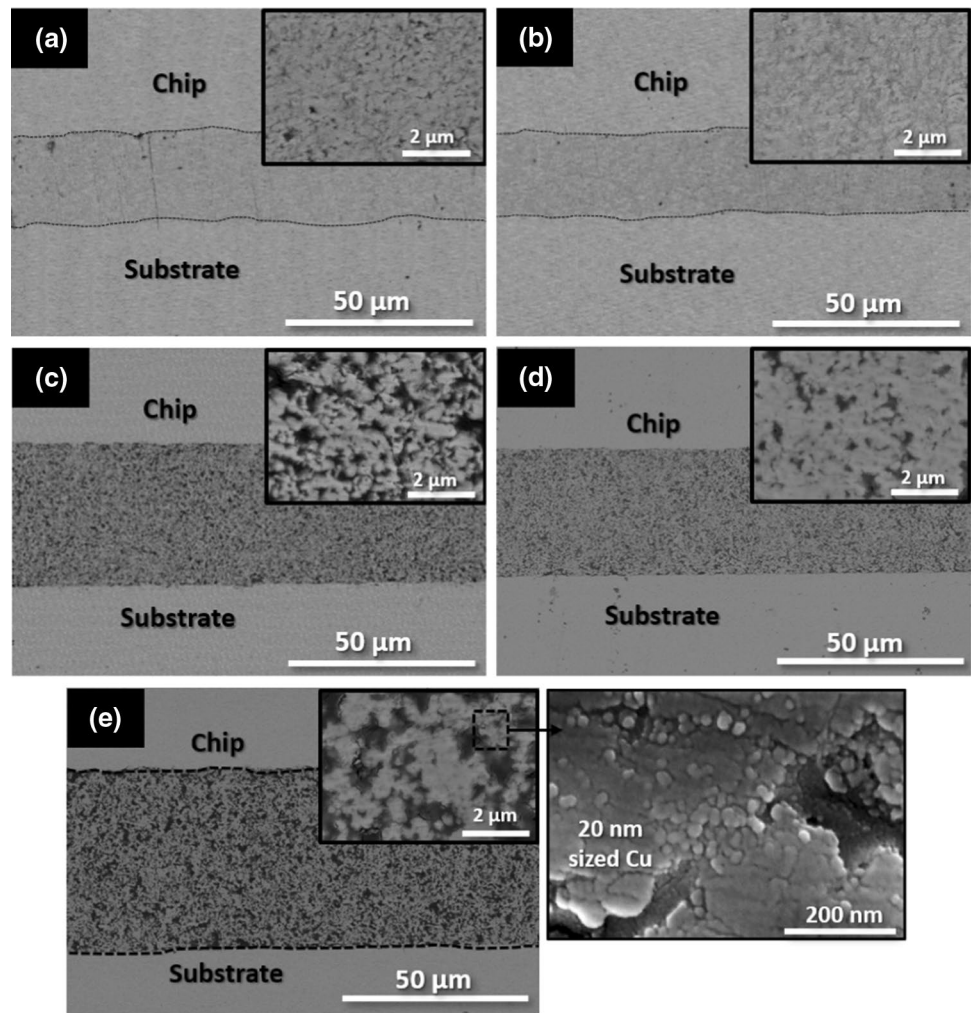


Fig. 4 **a** Shear strength and **b** XRD results of bondlines sinter-bonded with different pressure values, bonding temperatures, and times

well as high-temperature sustainability whether it contains slight oxidation or not.

The cross-sectional backscattered electron (BSE) images of the representative bondlines sinter-bonded for 60 s are shown in Fig. 5. The final thicknesses of bondlines in the low-magnification images, reduced from the printing thickness of 100 μm , indirectly reflect the sintering degree observed in the inset images (note that the black regions between sintered dendrites are voids). The sintering degree between the particles was identical even at the bondline/Cu finish interfaces. The dendritic shapes of initial Cu particles were barely noticeable in the bondlines. Moreover, it was determined that sintering degrees are proportional to the measured shear strength values. For example, the bondline sinter-bonded for 60 s at 300 °C under 10 MPa exhibited the highest density among the microstructures, as shown in Fig. 5b. To elucidate the effects generated by the reduction formulation, high-magnification observation among sparse

Fig. 5 Cross-sectional BSE images of bondlines sinter-bonded for 60 s at **a** 250 °C and **b** 300 °C under 10 MPa, at **c** 300 °C and **d** 350 °C under 5 MPa, and **e** at 350 °C under 2 MPa



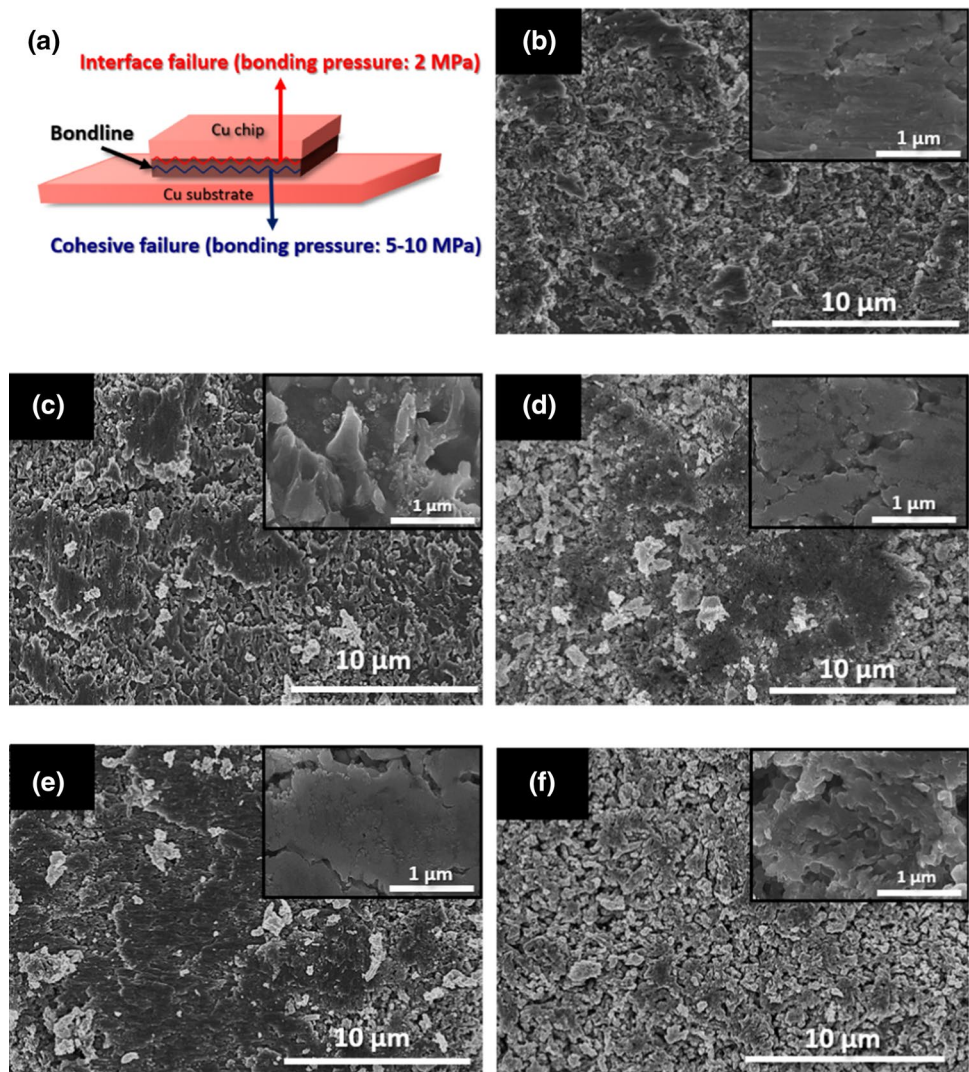
particles was attempted (inset of Fig. 5e). As a result, the formation of 200 nm-sized Cu particles was observed at the interfaces between particles due to reduction of the surface oxide layers on the Cu dendritic particles. The Cu nanoparticles between the dendritic particles may be an accelerating agent for sinter bonding. Concretely, most of the nanoparticles participated in and contributed to the sintering at 300 °C under 10 MPa (Fig. 5b), although they were partially sintered at 350 °C under 5 MPa (Fig. 5d).

The three main causes of the significantly rapid sinter bonding were bending deformation in the stems of Cu dendritic particles under pressure, outstandingly favorable sinterability of the nanonodules on the initial surfaces of particles, and formation of nanoparticles in between particles. The bending of stems can fill the large voids between particles, promptly eliminating them. Thus, higher bonding pressure is a crucial factor to attain more rapid sintering in this bonding technique using dendritic particles. Furthermore, the nano-sized surface nodules may exhibit rapid sintering behavior like nanoparticles at the contacts, which abruptly formed immediately after the bending deformation.

However, the surfaces of nanonodules easily oxidize during air heating for bonding. Nevertheless, the in situ reductions of the surfaces by a reduction formulation formed fresh Cu atoms, which were agglomerated into nanoparticles. The Cu nanoparticles on the surfaces act as a sintering accelerator under a strong synergy effect with the nano-sized nodules.

The fracture results of representative bondlines sinter-bonded for 60 s are presented in Fig. 6. The fracture surfaces of the bondlines sinter-bonded for 60 s at 250 °C (Fig. 6b) and 300 °C (Fig. 6c) under 10 MPa indicated the cohesive failure mode (Fig. 6a). Relatively dense sintering microstructures were observed in both surfaces, and shear bands (inset of Fig. 6b) and cup and cone fracture (inset of Fig. 6c), representative fracture microstructures in well-bonded metallic bondlines, were observed in the 250 and 300 °C surfaces, respectively. The bondlines sinter-bonded for 60 s at 300 °C (Fig. 6d) and 350 °C (Fig. 6e) under 5 MPa also showed the cohesive failure mode. It was also found in the fracture surfaces that Cu nanoparticles, which were reduced from the surface oxide of dendritic particles during heating, exist at the interfaces between Cu particles. However, the densities

Fig. 6 a Classification of fracture modes and fracture surface SEM images of bondlines sinter-bonded for 60 s at **b** 250 °C and **c** 300 °C under 10 MPa, at **d** 300 °C and **e** 350 °C under 5 MPa, and **f** at 350 °C with 2 MPa



of the bondlines decreased with decreased sintering, and shear bands were not observed. The bondline sinter-bonded under 2 MPa exhibited the interface failure mode (Fig. 6f), implying that the Cu finish/bondline interface was the weakest region due to the reduced sintering by deficient bending deformation. Contours of the Cu particles in the fracture surface can be distinguished with a large void fraction.

4 Conclusions

A novel pressure-assisted, die-attached method in air using Cu dendritic particles was successfully demonstrated under different combinations of bonding pressures and temperatures. The bonding pressure was a more dominant parameter than bonding time because it induces more contact between particles. It was determined that external pressure of at least 5 MPa effectively bends the stems of dendritic particles, filling the initial interparticulate voids. Immediately afterward,

the fresh Cu, reduced in situ at the nanonodules on the particle surfaces, provides significant sinterability under contact with neighboring particles. As a result, extremely rapid sinter bonding for 10 s at 300 °C was accomplished under 10 MPa. Although the pressure was decreased to 5 MPa, the 60 s sinter bonding at 350 °C exhibited a sufficient strength of 20.6 MPa, which surpasses the strength obtained using Pb–5Sn.

Acknowledgements This work was supported by the Materials & Components Technology Development Program (10080187) funded by the Ministry of Trade, Industry & Energy (MI, Korea).

References

1. J. Yan, G. Zou, Y. Zhang, J. Li, L. Liu, A. Wu, Y.N. Zhou, *Mater. Trans.* **54**, 879 (2013)
2. C.H. Lee, E.B. Choi, J.-H. Lee, *Scr. Mater.* **150**, 7 (2018)

3. P.G. Neudeck, R.S. Okojie, L.-Y. Chen, *Proc. IEEE* **90**, 1065 (2002)
4. H.S. Chin, K.Y. Cheong, A.B. Ismail, *Metall. Mater. Trans. B* **41**, 824 (2010)
5. K.S. Siow, Y.T. Lin, *J. Electron. Packag.* **138**, 020804 (2016)
6. S. Wang, M. Li, H. Ji, C. Wang, *Scr. Mater.* **69**, 789 (2013)
7. S. Fu, Y. Mei, G.-Q. Lu, X. Li, G. Chen, X. Chen, *Mater. Lett.* **128**, 42 (2014)
8. H. Zhang, C. Chen, J. Jiu, S. Nagao, K. Suganuma, *J. Mater. Sci. Mater. Electron.* **29**, 8854 (2018)
9. T. Ishizaki, R. Watanabe, *J. Mater. Chem.* **22**, 25198 (2012)
10. T. Yamakawa, T. Takemoto, M. Shimoda, H. Nishikawa, K. Shiokawa, N. Terada, *J. Electron. Mater.* **42**, 1260 (2013)
11. Y. Gao, H. Zhang, W. Li, J. Jiu, S. Nagao, T. Sugahara, K. Suganuma, *J. Electron. Mater.* **46**, 4575 (2017)
12. X. Liu, H. Nishikawa, *Scr. Mater.* **120**, 80 (2016)
13. J. Li, Q. Liang, T. Shi, J. Fan, B. Gong, C. Feng, J. Fan, G. Liao, Z. Tang, *J. Alloys Compd.* **772**, 793 (2019)
14. D. Ishikawa, H. Nakako, Y. Kawana, C. Sugama, M. Negishi, Y. Ejiri, S. Ueda, B.N. An, H. Wurst, B. Leyrer, T. Blank, M. Weber, in *Proceedings of 7th Electronic System-Integration Technology Conference (ESTC)*, IEEE, Dresden, (2018)
15. K. Suganuma, S.-J. Kim, K.-S. Kim, *JOM* **61**, 64 (2009)
16. J.H. Hwang, J.-H. Lee, *Met. Mater. Int.* **25**, 408 (2019)
17. W. Songping, M. Shuyuan, *Mater. Lett.* **60**, 2438 (2006)

Publisher's Note Springer Nature remains neutral with regard to jurisdictional claims in published maps and institutional affiliations.